Catal Lett (2012) 142:100–107
DOI 10.1007/s10562-011-0729-5

Synthesis and Catalytic Properties of Carbon-Nanotube-Supported RuO_2 Catalyst Encapsulated in Silica Coating

Hao Yu · Yingsi Wu · Feng Peng · Yan Zhang · Hongjuan Wang · Jian Yang

Received: 7 August 2011 / Accepted: 26 October 2011 / Published online: 4 November 2011

Abstract A carbon-nanotube-supported RuO_2 nanocatalyst encapsulated in thin silica layer was successfully synthesized. The prior formation of silica over RuO_2 nanoparticles effectively hindered catalyst aggregation at high temperatures. The significant improvement of the resistance to sintering and the catalytic selectivity were demonstrated in competitive oxidation of n-butanol and i-butanol and methanol oxidative dehydrogenation.

Keywords Ruthenium oxide · Silica · Aerobic oxidation · Oxidative dehydrogenation · Stability · Selectivity

1 Introduction

In the past decades, the conscious application of nanotechnology in catalysis field has allowed for fabricating various complex hybrid structures to control chemical reactions. Among the controllable complex structures, the catalysts with embedded phases have attracted extensive interests due to the facts: (i) the active sites embedded can be stabilized under harsh conditions; and (ii) the catalyst may exhibit enhanced activity benefited from the confinement effect [1, 2]. For examples, nanohybrids with porous shells and metal cores, e.g. $Au@ZrO_2$ [3], $Pd@SiO_2$ [4, 5], $Pt@SiO_2$ [6], Pt@C [7], $Ru@ZrO_2$ [8], Rh@C [9], $Rh@Al_2O_3$ [10], $Ni@SiO_2$ [11], can be synthesized by various methods, over which the prolonged durability and enhanced activity in diverse reactions have been proved. The relative large metal-support interface area in $CuO_x@TiO_2$ can favor the photocatalytic activity, due to the reduction of the band gap [12]. Takenaka et al. have coated silica over carbon nanotube (CNT) supported Pt catalysts [13, 14]. The resultant catalysts showed excellent resistance against sintering in methane combustion [14] and leaching in electrocatalysis [15].

The porous coating layer plays diverse roles in the embedded/encapsulated catalysts. On one hand, the catalyst can be stabilized by preventing them from aggregation. On the other hand, although the coating acts as a barrier layer hindering the accessibility of reactants, the activity could be enhanced due to the resistance to sintering or leaching [4], and the unique metal-support interaction [16]. It is worth mentioning that the peculiar strong metal-support interaction of these materials may result in electronic deactivation. For instance, although ceria coated noble metals ($Au@CeO_2$ and $Pd@CeO_2$) are active [17, 18], $Pd@CeO_2$ suffers from fast deactivation under reducing condition [19].

Hitherto, few reports concern on the alteration of reaction selectivity via the porous coating. Cortial et al. [20] reported an improved selectivity toward the linear product of allylic amination of cinnamyl acetate by benzylamine over $Pd@SiO_2$. Wada et al. [21] observed a size selectivity of reactants in the aerobic oxidation of alcohols over $Pd/TiO_2@SiO_2$. These results suggested that reaction selectivity could be tuned by the porous coating.

In this study, we encapsulated RuO_2/CNT, an efficient catalyst for aerobic oxidation of alcohols and methanol oxidative dehydrogenation (ODH) [22–24], within a thin silica layer. The activity, stability and selectivity of the resulting $RuO_2/CNT@SiO_2$ catalyst were tested with these two probing reactions. The special attention was focused

H. Yu (✉) · Y. Wu · F. Peng · Y. Zhang · H. Wang · J. Yang
School of Chemistry and Chemical Engineering, South China University of Technology, Guangzhou 510640, People's Republic of China
e-mail: yuhao@scut.edu.cn

on the catalyst stability and possibility of controlling the selectivity.

2 Experimental

2.1 Synthesis of Catalysts

The RuO_2/CNT (Multi-walled CNTs, Shenzhen Nanotech Port Co. Ltd.) catalyst was prepared by a H_2O_2 homogeneous oxidation precipitation (HOP) method as reported elsewhere [22]. 10% nominal RuO_2 loading, showing the highest activity in aerobic oxidation of benzyl alcohol [23], was used in this work. To coat silica over RuO_2/CNT, 0.5 g RuO_2/CNT were dispersed in 12.5 mL 3-aminopropyltriethanoxysilane (APTES, 99%, Alfa Aesar Co. Ltd.) by ultrasonication for 2 h. The suspension was added into a mixture of 400 mL absolute ethanol and 1.75 mL tetraethoxysilane (TEOS, 98%, Aldrich) with stirring for 3 h at 5 °C. Then 1 ml NH_4OH was injected into the suspension with vigorous stirring at 5 °C for 6 h. The solids obtained were washed with ethanol thoroughly and annealed in air or N_2 at 300–400 °C for 2 h. The resulting catalysts were denoted as RuO_2/CNT@SiO_2.

2.2 Catalyst Characterizations

The composition of RuO_2/CNT@SiO_2 catalyst was assessed by the combination of TGA (Netzsch, STA449C) and Electron Probe Micro-Analysis (Shimadzu, EPMA-1600). The weight percentage of CNTs was determined by burning 5–10 mg sample in TGA in air with a flow rate of 25 mL/min ramping at 10 °C/min. The Si:Ru atomic ratio (R) of catalyst was measured with EPMA.

The catalysts were characterized by N_2 adsorption (Micrometrics ASAP 2010), SEM (JEOL, JSM-7401), TEM (JEOL, JEM-2010/2010F), XPS (Kratos, Axis Ultra DLD), H_2-Temperature Programmed Reduction and CO chemisorption (Micromeritics, Auto Chem II Chemisorption Analyzer). The Transmission Electron Microscope was operated at an acceleration voltage of 200 kV and equipped with an Energy Dispersive Spectrometer (Oxford Instruments). The XPS spectra were obtained using the radiation of AlKa line as the excitation source. The calibration was conducted by referring the C1s signal to the binding energy of 284.6 eV. For the quantitative analysis of surface atom concentration, Wagner sensitivity factors were used and the background was subtracted with Shirley-type baseline. Before H_2-TPR experiments, 0.05 g catalyst was pretreated in air at 120 °C for 0.5 h. Then the TPR profile was recorded at a ramping rate of 10 °C min^{-1} under flowing H_2(10%)/Ar at 50 N cm^3 min^{-1}. The dispersion of RuO_2 domains was evaluated by measuring the dispersion of Ru crystallites using CO chemisorption at 100 °C after reducing RuO_2 in H_2 at 300 °C for 30 min and purging with He for 1 h. In this work, CO chemisorption was used to obtain a relative measurement for the dispersion of metal, because RuO_2 had to be reduced to Ru^0 for the measurement, which may result in particle aggregation or carbon gasification due to H_2 spillover. Our previous work has demonstrated that the reduction process would not change the relative tendency of dispersion of RuO_2 [23]. We also assumed that the carbon gasification effect was minor below 300 °C, since such an effect usually occurs above 500 °C for Ru–C system [25, 26].

2.3 Catalytic Tests

The liquid-phase oxidation reaction was carried out in a one port flask with a condenser. 0.1 g catalyst was added first, then 1 mmol n-butanol, 1 mmol i-butanol and 5 mL toluene as solvent were added to form a homogenous suspension under strong mechanical stirring. Then, oxygen was bubbled into the suspension at 10 mL/min. Meanwhile, the system was heated and reached 80 °C within 10 min. The reaction was conducted at 80 °C under ambient pressure for 2 h. The liquid products were analyzed by an Agilent 6820 Gas Chromatographer.

The methanol ODH was carried out in a quartz fixed bed reactor with i.d. of 7 mm at ambient pressure and at 120 °C [24]. The catalysts were diluted with 0.4 g silica. The partial pressures of methanol and O_2 were 7 and 20 kPa, respectively. The effect of external mass transfer has been excluded under the experimental conditions used in this study. The effect of internal diffusion was minimized by using the as-prepared fine catalyst powder. The effluent gas was analyzed by a gas chromatographer equipped with a TCD detector and a FID detector.

3 Results and Discussion

The RuO_2/CNT@SiO_2 nanohybrids were prepared by using APTES as a coupling layer and TEOS as a hydrolytic reagent [27, 28], as the process interpreted in Fig. 1. The –COOH groups on CNTs serve as the sites for anchoring RuO_2 nanoparticles, leaving–OH, –C=O and epoxide on CNT surfaces [24, 29]. The RuO_2 nanoparticles are highly hydrous and rich in surface hydroxyls [23, 30]. The reaction between hydroxyls and APTES gives amine groups terminated RuO_2/CNT. TEOS strongly interacts with the basic amine groups with an assist from NH_4OH, resulting in a hydrolysis of TEOS and the formation of silica layers. Annealing is important to fully develop porous silica layers. As shown in Table 1, the Brunauer–Emmett–Teller surface area of RuO_2/CNT@SiO_2 without annealing was

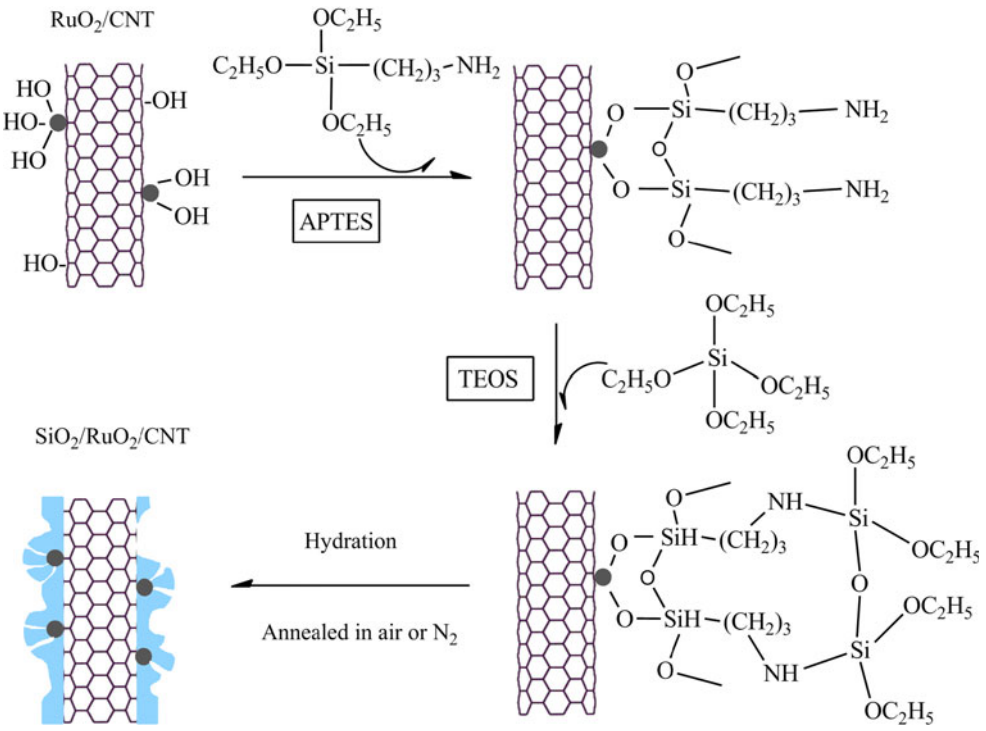

Fig. 1 Schematic mechanism of coating SiO_2 layer over RuO_2/CNT

Table 1 BET surface area of the samples used in this work

Catalyst	CNTs	RuO_2/CNT			RuO_2/CNT@SiO_2		
Pre-treatment	–[a]	–[a]	Air, 300 °C	N_2, 400 °C	–[a]	Air, 300 °C	N_2, 400 °C
$S_{BET}/m^2/g$	164	162	157	159	110	163	125

[a] Simply dried in air at 110 °C

110 m^2/g, while it was significantly increased to 163 and 125 m^2/g by annealing in air or N_2, respectively. It was also proved that the catalyst without annealing is inactive in the probing reactions.

Figure 2a shows the SEM image of RuO_2/CNT@SiO_2 annealed in N_2. The fibrous structure was clearly observed and no silica aggregates were found in SEM. Compared with its counterpart without silica coating (Fig. 2b), a thin and homogenous silica layer with amorphous structure can be observed in TEM (Fig. 2c–e). The EDS analysis indicated the existence of Si and Ru. The average thickness of silica layer over RuO_2/CNT@SiO_2 is less than 5 nm. Such a thin coating can minimize the diffusion resistance of reactant in a catalytic application. Figure 2d, e shows RuO_2 nanoparticles encapsulated by silica layer with thickness of about 2 nm, evidencing that the catalytic particles are successfully coated by silica. It is noteworthy that the size distribution of RuO_2 nanoparticles did not change notably after coating with silica. The average RuO_2 sizes of RuO_2/CNT and RuO_2/CNT@SiO_2 are 1.5 ± 0.4 and 1.4 ± 0.7 nm, respectively. Also, no agglomeration among the nanoparticles was observed in RuO_2/CNT@SiO_2.

Figure 3 presents the survey and high-resolution Ru XPS spectra of the catalysts with and without SiO_2 coating. Compared with RuO_2/CNT, the Ru 3d and Ru 3p signals of RuO_2/CNT@SiO_2 almost disappeared, indicating that RuO_2 is completely coated. As shown in Table 2, the Ru content was reduced from 2.4% to 0.1%, around the detection limit of XPS. However, the surface carbon percentage of RuO_2/CNT@SiO_2 reduced little compared to RuO_2/CNT, implying that the silica coating on CNT surfaces is either thin or discontinuous. It can be explained by the reaction mechanism between APTES and RuO_2/CNT. With the nitric acid oxidation method, the content of –OH groups in CNTs was about 0.67 mmol/g [29]. The domains without –OH sites might be coated with less silica. Compared with functionalized CNTs, the surfaces of RuO_2 nanoparticles are richer in hydroxyls. The water content may be high up to 5.2 water molecules per Ru atom [23]. Hence, the reaction between APTES and RuO_2/CNT tends to take place on the RuO_2 nanodomains, resulting in a preferencial deposition of silica over RuO_2 and leaving CNT surfaces partically exposed. Acturally, we indeed observed bare CNT surfaces without silica layer but with

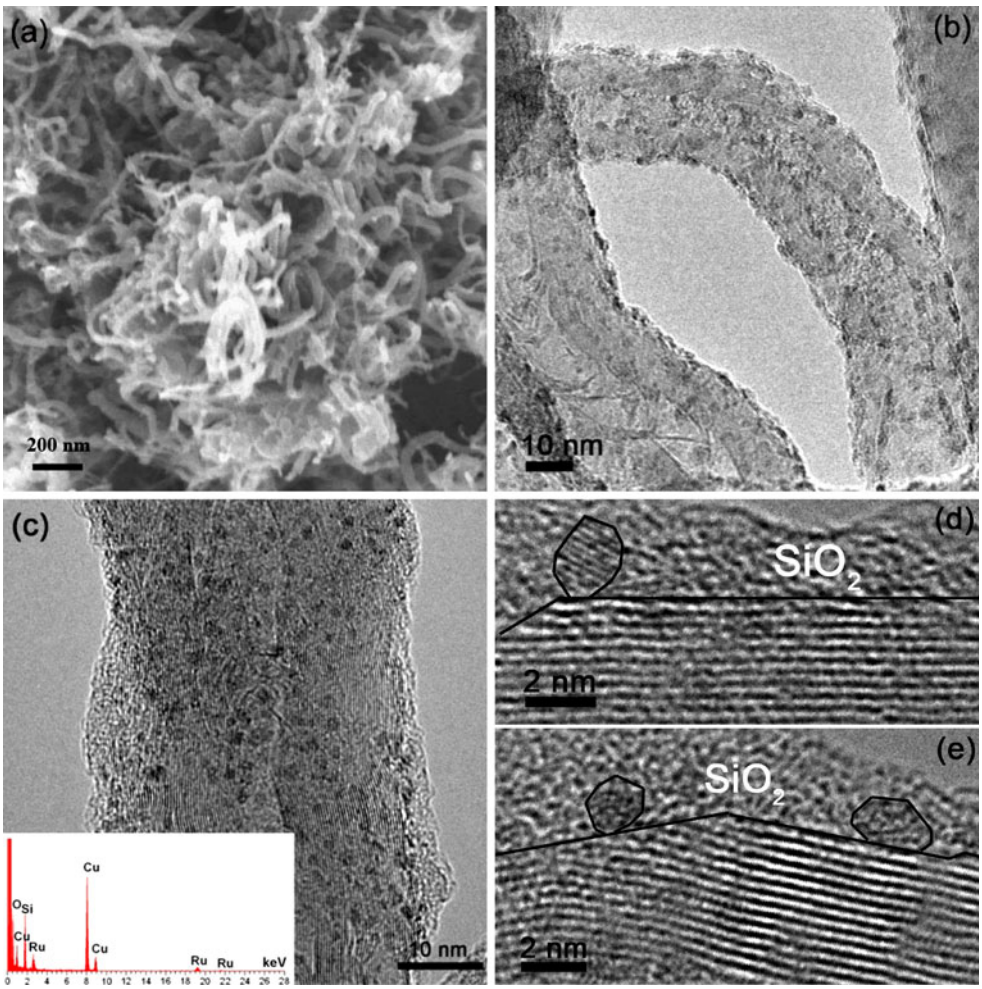

Fig. 2 SEM (**a**) and TEM (**b**–**e**) images of RuO_2/CNT@SiO_2 (**a**, **c**, **d**, **e**) and RuO_2/CNT (**b**). The inset of (**c**) shows the EDS spectrum of the RuO_2/CNT@SiO_2 sample

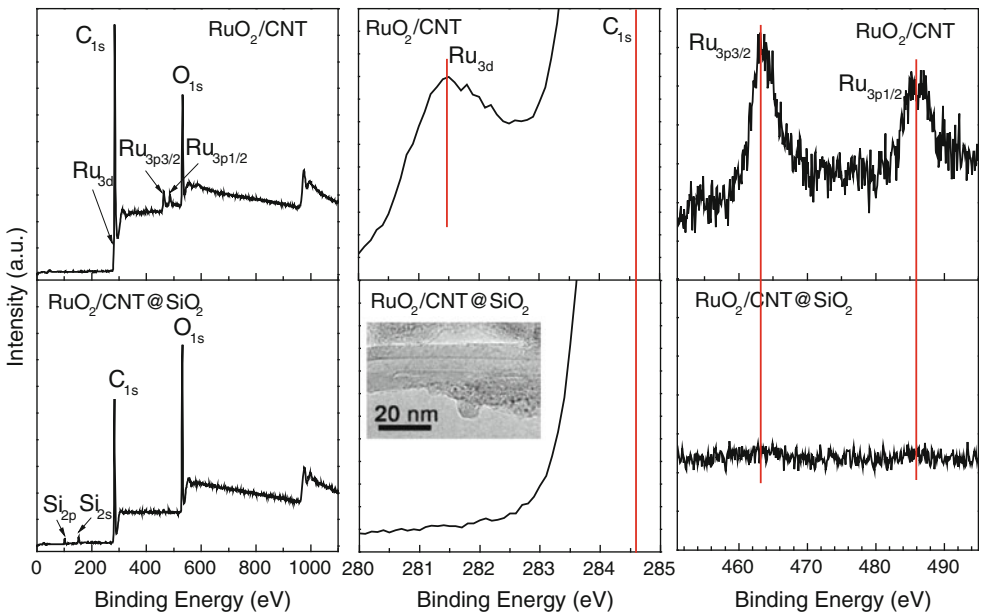

Fig. 3 Survey (*left*), Ru 3d (*middle*) and Ru 3p (*right*) XPS spectra of RuO_2/CNT (*upper panel*) and RuO_2/CNT@SiO_2 (*lower panel*). The inset for the Ru 3d spectrum of RuO_2/CNT@SiO_2 shows the prior coating of silica over RuO_2 particles

Table 2 Compositions of RuO_2/CNT and RuO_2/CNT@SiO_2 catalysts on surfaces and in bulk

Catalyst[a]	Hydrolysis/h	Surface[b]/at%				Bulk[c]/wt%	
		C	O	Ru	Si	SiO_2	RuO_2
RuO_2/CNT	–	77.8	19.7	2.5	0	0	14.9
RuO_2/CNT@SiO_2	6	73.6	20.9	0.1	5.4	13.4	13.6

[a] Annealed in N_2 at 300 °C

[b] By XPS

[c] By the combination of TGA and EPMA

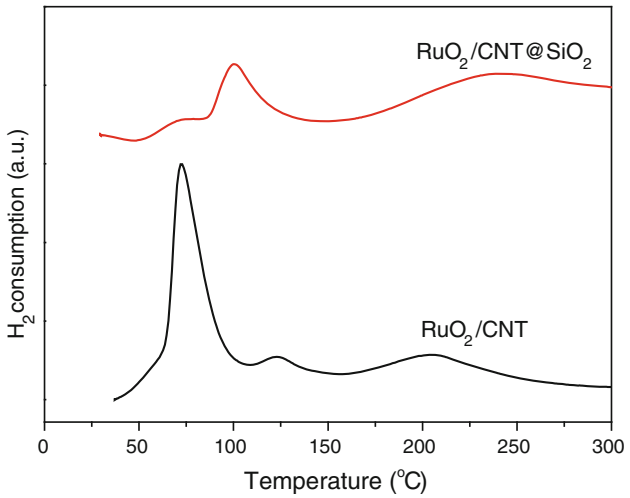

Fig. 4 H_2-TPR profiles of RuO_2/CNT and RuO_2/CNT@SiO_2 catalysts. The RuO_2/CNT@SiO_2 sample was prepared with a hydrolysis time of TEOS for 6 h

highly crystalline tubular walls, while the RuO_2 nanoparticles nearby are encapsulated by silica, as shown in the inset of Fig. 3.

The silica coating changed the reducibility of RuO_2/CNT, as shown in the TPR profiles in Fig. 4. Without the silica layer, RuO_2 would be reduced at about 80 °C. However, the main reduction peaks of RuO_2/CNT@SiO_2 shifted to around 100 °C, meanwhile the reduction peaks between 200 and 300 °C were enhanced markedly, indicating the lower reducibility due to the diffusion resistance through the micropores in SiO_2 layers.

The competitive oxidation between n-butanol and i-butanol was used to investigate the properties of RuO_2/CNT@SiO_2 catalyst (Table 3). Since the silica layer provides a porous barrier layer for the catalytic domains, the selectivity may be changed through the sieving effect. Thus, i-butanol with the higher steric hindrance than n-butanol will be more difficult to be transported through micropores, leading to a selective oxidation of the isomers.

As the RuO_2/CNT annealed in air at 300 °C, the oxidation rates of n-butanol and i-butanol were quite low, being 0.14 and 0.08 mol mol^{-1}_{RuO2} h^{-1}, respectively. However, when the silica layer was coated, the reaction rates of n-butanol were markedly improved by over 2 folds, achieving 0.41 mol mol^{-1}_{RuO2} h^{-1} for RuO_2/CNT@SiO_2. It can be explained by the high resistance to sintering of RuO_2 particles in RuO_2/CNT@SiO_2. Due to the weak interaction between RuO_2 and CNTs and the unstable amorphous structure of hydrous RuO_2, the RuO_2 nanoparticles on CNTs tend to aggregate in oxidative atmosphere at elevated temperatures [24, 31], as shown in Fig. 5a. On the other hand, the oxidation of CNT support in air may lead to the gasification of CNT defects [32], especially with the catalysis of RuO_2 [24]. Although the oxidation had little effect on catalyst weight under 300 °C, the structural changes near RuO_2 nanoparticles may favor to the aggregation of RuO_2. After coating a silica layer, the

Table 3 Activities and selectivities of the competitive oxidation of n-butanol (*n*) and i-butanol (*i*)

Catalyst	Dispersion (%)	Conversion (%)		Conversion rate (mol mol^{-1}_{RuO2} h^{-1})		TOF[a] (mol mol^{-1}_{RuO2} h^{-1})		Selectivity[b]
		n	*i*	*n*	*i*	*n*	*i*	
RuO_2/CNT[c]	–	3.17	1.80	0.14	0.08	–	–	1.8
RuO_2/CNT@SiO_2[c]	–	8.30	3.33	0.41	0.16	–	–	2.5
RuO_2/CNT[d]	18.2	15.9	6.50	0.71	0.29	3.9	1.6	2.5
RuO_2/CNT@SiO_2[d]	9.6	11.45	3.45	0.56	0.17	5.8	1.8	3.4

[a] Turnover frequency per Ru atom on surface

[b] Defined as the ratio of consumption rates of n-butanol and i-butanol

[c] Annealed in air at 300 °C

[d] Annealed in N_2 at 400 °C

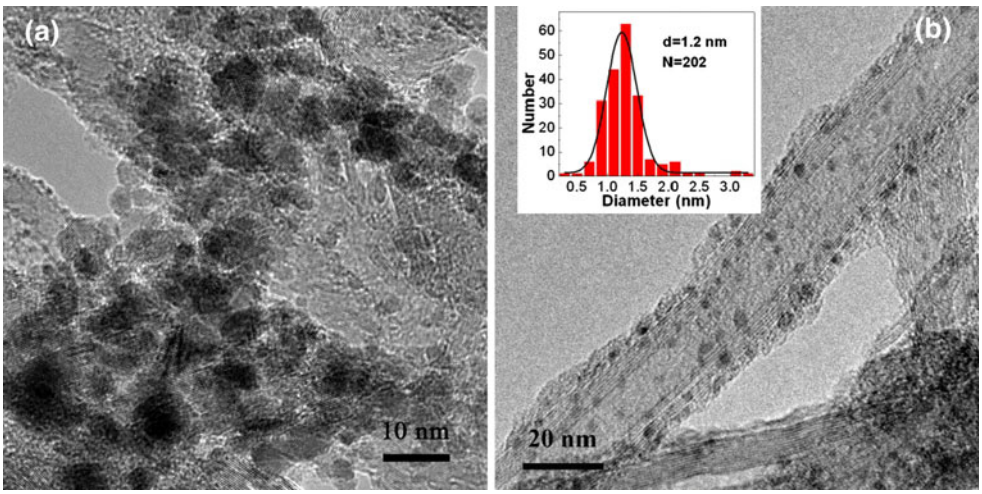

Fig. 5 TEM images of RuO_2/CNT (**a**) and RuO_2/CNT@SiO_2 (**b**) annealed in air at 300 °C. The inset of (**b**) shows the histogram of RuO_2 particle size distribution

aggregation was dramatically suppressed, as shown in Fig. 5b. The average size of RuO_2 nanoparticles (1.2 ± 0.6 nm, by TEM) did not change after annealed in air at 300 °C when the catalyst was coated with SiO_2, resulting in the high activity of RuO_2/CNT@SiO_2. Although the silica layer increased the diffusion resistance of the reactants, the activity of RuO_2/CNT@SiO_2 was superior to the catalyst without silica layer.

A further improvement of the activity and selectivity was achieved over the catalyst annealed in N_2. Since the RuO_2/CNT catalyst annealed in N_2 at 400 °C maintained the small particle size (1.7 ± 0.5 nm) [24], the higher activity and selectivity were achieved. With the silica coating, the reaction rates of n-butanol and i-butanol decreased. It is interesting that the TOF of RuO_2/CNT@SiO_2 for n-butanol was higher than that of RuO_2/CNT, while the TOF for i-butanol changed little, indicating a selective enhancement of activity for linear reactant. These results indicated that the selectivity can be tuned by the additional diffusion resistance through the silica layer, which may be utilized to selectively catalyze the certain substance in mixture.

Except for the selective accessibility of reactants, it can be also expected that the product distribution will be changed when products with different sizes are formed. The methanol ODH produces value-added oxygenated compounds, e.g. formaldehyde (HCHO, FA), methylformate ($HCOOCH_3$, MF) and dimethoxymethane (CH_3O-CH_2OCH_3, DMM), as shown in Scheme 1 [33, 34]. It is noteworthy that the surface functional groups such as C=O and C–OH may be active for the ODH reaction, as demonstrated in ODH of alkanes, ethylbenzene [35, 36] and oxidation of acrolein [37]. However, in this work, we attributed the catalysis to RuO_2 because the conversion over bare CNT supports were very low and the reaction temperature was so low that carbon was unlikely to play a significant catalytic role.

The conversions and selectivity patterns of methanol ODH reaction over RuO_2/CNT and RuO_2/CNT@SiO_2 are shown in Fig. 6. The initial conversion of methanol was both controlled at about 25% by tuning the space velocity. Significant change of activity vs. time-on-stream was observed over RuO_2/CNT. After the first hour, the methanol conversion increased to over 50%. It is probably due to the re-hydration of RuO_2 surface by the water formed, for the activity of RuO_2/CNT depends on the amount of structural water of RuO_2. Subsequently, the conversion decreased gradually to 40% within ~4 h, probably caused by the aggregation in oxidative atmosphere. In a long term test, a stable methanol conversion of 32% has been achieved after 33 h. Meanwhile, a selectivity pattern of 14.2% FA, 29.6% MF and 56.2% DMM was measured. In contrast to the instability of RuO_2/CNT, a stable ODH reaction was achieved over RuO_2/CNT@SiO_2. Only 3% decrease of conversion (from 26 to 23%) was observed during 250 min on stream.

The silica layer influenced the product selectivity significantly. Under the similar conversion level, the RuO_2/

Scheme 1 Oxidative dehydrogenation of methanol

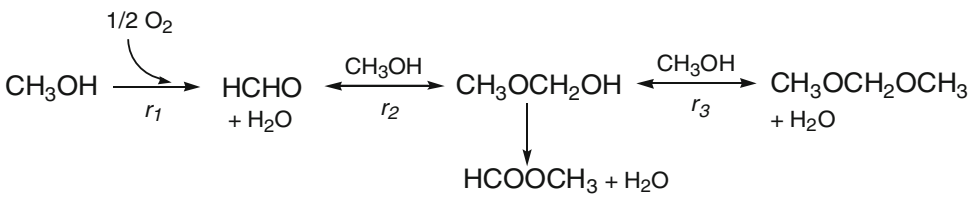

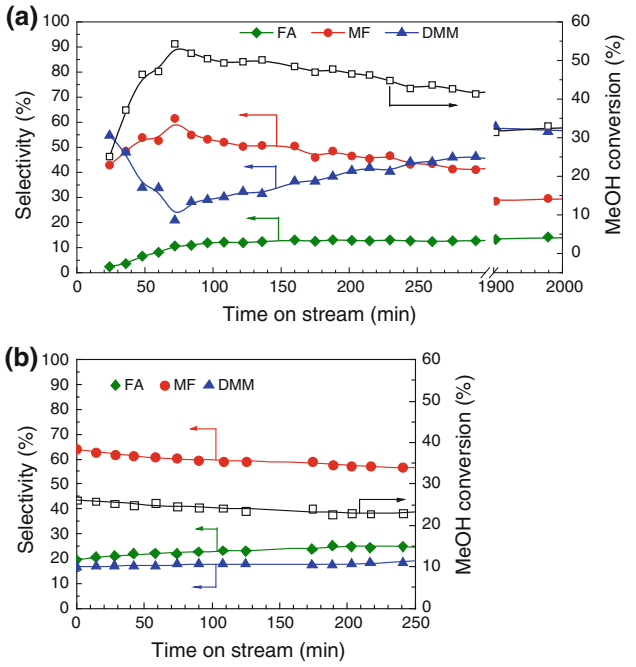

Fig. 6 Conversions and selectivity patterns of methanol ODH reaction over (**a**) RuO_2/CNT and (**b**) RuO_2/CNT@SiO_2. The gas hourly space velocities were (**a**) 60000 and (**b**) 36000 N cm^3 g^{-1} h^{-1}

CNT@SiO_2 catalyst gave much higher selectivities toward MF (~60%) and FA (~25%), while the selectivity of DMM decreased to 15%. Over RuO_2/CNT, the formation of FA, MF and DMM depends on the reactant residence time and acidity of the active sites [34]. The high selectivity of DMM indicated the high accessibility and strong adsorption of methanol over RuO_2/CNT, since three methanol molecules are required to produce one DMM molecule. The formation of DMM would be suppressed by hindering the diffusion of methanol. Hence, the selectivity of DMM reduced when the porous barrier layer was introduced, which limited the accessibility of methanol, resulting in a preferential production of MF. These results display an interesting approach to control the product distribution to obtain desired oxygenated derivates of methanol.

4 Conclusions

In summary, a RuO_2/CNT catalyst was successfully coated by a thin silica layer (<5 nm). The SiO_2 layer was preferentially deposited on RuO_2 nanoparticles and effectively prevented the aggregation among the nanoparticles. The porous SiO_2 layer increased the selectivity of n-butanol in its competitive aerobic oxidation with i-butanol. The RuO_2/CNT@SiO_2 catalyst also exhibited the possibility to control the product distribution of the methanol ODH reaction, offering a preferential production of MF. The catalytic results demonstrate a conceptual design of nanohybrid catalyst with high stability and controllable reaction selectivity via the porous SiO_2 coating.

Acknowledgments We acknowledge the financial support from the National Science Foundation of China (No. 20806027), the Guangdong Provincial Science and Technology Project (No. 2006A10903002) and Guangzhou Civic Science and Technology Project (No. 2007Z3-D2101).

References

1. De Rogatis L, Cargnello M, Gombac V, Lorenzut B, Montini T, Fornasiero P (2010) ChemSusChem 3:24
2. Mori K, Yamashita H (2010) Phys Chem Chem Phys 12:14420
3. Arnal PM, Comotti M, Schüth F (2006) Angew Chem Int Ed 45:8224
4. Park JN, Forman AJ, Tang W, Cheng JH, Hu YS, Lin HF, McFarland EW (2008) Small 4:1694
5. Takenaka S, Susuki N, Miyamoto H, Tanabe E, Matsunea H, Kishida M (2010) Chem Commun 46:8950
6. Joo SH, Park JY, Tsung CK, Yamada Y, Yang PD, Somorjai GA (2009) Nat Mater 8:126
7. Ng YH, Ikeda S, Harada T, Sakata T, Mori H, Takaoka A, Matsumura M (2008) Langmuir 24:6307
8. Lorenzut B, Montini T, Pavel CC, Comotti M, Vizza F, Bianchini C, Fornasiero P (2010) ChemCatChem 2:1096
9. Harada T, Ikeda S, Ng YH, Sakata T, Mori H, Torimoto T, Matsumura M (2008) Adv Funct Mater 18:2190
10. Montini T, Condo AM, Hickey N, Lovey FC, De Rogatis L, Fornasiero P, Graziani M (2007) Appl Catal B Environ 73:84
11. Takenaka S, Umebayashi H, Tanabe E, Matsune H, Kishida M (2007) J Catal 245:392
12. Gombac V, Sordelli L, Montini T, Delgado JJ, Adamski A, Adami G, Cargnello M, Bernal S, Fornasiero P (2010) J Phys Chem A 114:3916
13. Takenaka S, Arike T, Nakagawa K, Matsune H, Tanabe E, Kishida M (2008) Carbon 46:365
14. Takenaka S, Arike T, Matsune H, Tanabe E, Kishida M (2008) J Catal 257:345
15. Takenaka S, Matsumori H, Nakagawa K, Matsune H, Tanabe E, Kishida M (2007) J Phys Chem C 111:15133
16. Yeung CMY, Yu KMK, Fu QJ, Thompsett D, Petch MI, Tsang SC (2005) J Am Chem Soc 127:18010
17. Cargnello M, Gentilini C, Montini T, Fonda E, Mehraeen S, Chi MF, Herrera-Collado M, Browning ND, Polizzi S, Pasquato L, Fornasiero P (2010) Chem Mater 22:4335
18. Cargnello M, Wieder NL, Montini T, Gorte RJ, Fornasiero P (2010) J Am Chem Soc 132:1402
19. Wieder NL, Cargnello M, Bakhmutsky K, Montini T, Fornasiero P, Gorte RJ (2011) J Phy Chem C 115:915
20. Cortial G, Siutkowski M, Goettmann F, Moores A, Boissiere C, Grosso D, Le Floch P, Sanchez C (2006) Small 2:1042
21. Wada K, Yano K, Kondo T, Mitsudo T (2006) Catal Today 117:242
22. Fu XB, Yu H, Peng F, Wang HJ, Qian Y (2007) Appl Catal A Gen 321:190
23. Yu H, Fu XB, Zhou CM, Peng F, Wang HJ, Yang J (2009) Chem Commun 2408
24. Yu H, Zeng K, Fu XB, Zhang Y, Peng F, Wang HJ, Yang J (2008) J Phy Chem C 112:11875
25. Guerrero-Ruiz A, Badenes P, Rodríguez-Ramos I (1998) Appl Catal A Gen 173:313

26. Xiong K, Li J, Liew K, Zhan X (2010) Appl Catal A Gen 389:173
27. Kim M, Hong J, Lee J, Hong CK, Shim SE (2008) J Colloid Interface Sci 322:321
28. Fu Q, Lu C, Liu J (2002) Nano Lett 2:329
29. Peng DF, Yu H, Peng F, Wang HJ, Yang J (2009) Chin J Catal 30:570
30. Yu H, Zhang Y, Fu XB, Peng F, Wang HJ, Yang J (2009) Catal Commun 10:1752
31. Chang KH, Hu CC (2006) Appl Phys Lett 88:193102
32. Frank B, Rinaldi A, Blume R, Schlogl R, Su DS (2010) Chem Mater 22:4462
33. Liu H, Iglesia E (2005) J Phys Chem B 109:2155
34. Tatibouet JM (1997) Appl Catal A Gen 148:213
35. Frank B, Morassutto M, Schomacker R, Schlogl R, Su DS (2010) ChemCatChem 2:644
36. Rinaldi A, Zhang J, Frank B, Su DS, Hamid SBA, Schlogl R (2010) ChemSusChem 3:254
37. Frank B, Blume R, Rinaldi A, Trunschke A, Schlögl R (2011) Angew Chem Int Ed 50:10226